Ag nanoparticles decorated ZnO tip-likenanowire for improving gas sensing applications

A. Ramos-Carrazco[a], J. V. Lopez-Fernandez[a], R. Rangel-Segura[b], J. R. Noriega[a], D. Berman-Mendoza[a,c], R. Garcia-Gutierrez[a], A. Vera-Marquina[a], R. Gomez-Fuentes[a], G. Valenzuela-Hernandez[a,c,*]

[a]*Department of Physics Research, University of Sonora, Hermosillo, Sonora, Mexico.*

[b]*Faculty of Chemical Engineering, Michoacan University San Nicolas de Hidalgo, Morelia, Michoacán, Mexico.*

[c]*Department of Physics, University of Sonora, Hermosillo, Sonora, Mexico.*

The growth of Ag NPs decorated ZnO tip-like nanowires was obtained by a combination of the chemical vapor deposition and the micro-spraying methods. ZnO growth was analyzed by a two-level factorial experimental design with temperature, pressure, and zinc mass as the main parameters. The process of Ag NPs synthesis by electrolysis and their transport to the semiconductor surface using micro-spraying is presented in detail. By means of electrical and X-ray photoelectron spectroscopy, the potential of Ag NPs decorated ZnO tip-like nanowires to be used an active layer in gas sensor is demonstrated.

(Received March 31, 2023; Accepted June 9, 2023)

Keywords: Zinc oxide, Silver nanoparticles, Chemical vapor deposition, Gas sensor

1. Introduction

The increasing levels of pollution, which has resulted from our contemporary lifestyles, has increased the demand for sensors. Several devices have been used to meet the demands of modern society, with an emphasis on chemiresistive sensors [1]. These devices use materials that can detect changes in their environment based on variations in their properties. Zinc oxide (ZnO) has been one strong candidate to be applied in sensors because of their high sensitivity, easy fabrication methods, low cost, ultraviolet photoresponse, and high compatibility with other semiconductor manufacture processes [2–5]. Particularly, the performance of ZnO based-sensing devices strongly depend on their dimensions and shape. 1D ZnO structures, like nanorods, nanobelts, nanotubes, nanowires, have been recently explored [6,7]. Due to their physical properties and potential applications, low-dimensional ZnO materials have been explored for nanosensors applications. Also, one-dimensional ZnO structures have been widely used in the development of gas sensors due to the physicochemical stability of the semiconductor and its thermal stability under different working environment [8–10]. Furthermore, the reduction in the structure dimensions increases the effective area of the nanostructure, hence an improved performance of the gas sensor compared to conventional sensors. Therefore, the growth of ZnO structures in the nanometric scale, is very important for the development of novel technologies.

Different techniques have been applied to synthesize 1D ZnO structures such as molecular beam epitaxy (MBE), pulse laser deposition (PLD), and chemical vapor deposition (CVD) [11–13]. This latter is very attractive as a simple cost-effective means of producing a variety of ZnO morphologies [14]. ZnO nanowires (NWs) have been reported using different tube chambers that require metals like Au and AuZn alloy as catalysts, in the presence of oxygen gas [15–17]. Also, the synthesis of ZnO NWs catalyst-free using CVD is still in debate due to the important role of growth conditions, such as reactor geometry, temperature, pressure, and carrier gas flow [13].

*Corresponding author: gerardo.valenzuela@unison.mx
https://doi.org/10.15251/JOR.2023.193.331

However, ideal conditions to obtain consistent and reproducible nanowires are complex and depends on the used operational parameters of the instruments and equipment.

Recently, the functionalization of the surface of the ZnO nanostructures has been explored using noble-metal nanoparticles. Due to the charge interaction between nanoparticles and the semiconductor, the enhancement in the response of the ZnO-based gas sensors has attracted the interest in electronics materials research [18,19]. Noble-metal nanoparticles are commonly implemented in ZnO for gas sensing applications, particularly silver and gold NPs. Currently, the coupling between Ag NPs and ZnO nanostructure have attract the attention for gas sensing applications due to charge transfer based on redox reaction [20].

In this work, ZnO tip-like nanowires (T-NWs) without catalyst were deposited by tuning the operational parameters of a chemical vapor deposition equipment, being adjusted to high temperature and low pressure. Cathodoluminescence (CL) and X-ray photoelectron spectroscopy (XPS) results indicate the characteristic emission of ZnO and the conventional stoichiometry in the obtained ZnO T-NWs. By means of an electrolysis system, the synthesis and size control of silver nanoparticles (Ag NPs) were accomplished. The nanoparticles exhibits the characteristic plasmon resonance at 413 nm and a linear tendency in particle size as function of the supplied voltage. The decoration of the ZnO surface with Ag NPs was obtained with a micro-spraying system. SEM images corroborates the presence of the incorporated Ag NPs on the ZnO T-NWs surface. On further analysis, electrical and XPS characterization evidences the interaction between Ag NPs and ZnO, increasing the electrical response of the semiconductor by means of a redox reaction. The Ag NPs decorated ZnO T-NWs here in presented are suitable for gas sensing application due to the sensitivity in electrical response.

2. Experimental

2.1. ZnO synthesis by chemical vapor deposition

The CVD reactor used in this study consist of a quartz tube placed in a furnace with one heating zone capable of reaching 1200 °C. This reactor has 25 mm external diameter, 2 mm thickness and 304 mm length. To provide vapor reaction, oxygen cylinders (99.99 %) and nitrogen (99.999 %) gases were connected to the CVD inlets and high purity Zn microtraces (150 μm) were used as metallic precursor. A 2^3 factorial design was implemented using the following growth parameters: temperature, pressure, and mass of Zn, as shown in Table 1. The equipment herein used provides suitable conditions to control each parameter using a PID control for temperature, vacuum sensor for pressure, and Ohaus analytical balance with a readability of 0.0001 g, for Zn weighing. Nitrogen and oxygen flows were set up as 200 sccm and 75 sccm, respectively. The reaction was sustained during 30 min until Zn precursor was completely evaporated. Then, the furnace was set up to cool down to room temperature under N_2 flow. The corresponding synthesized sample was removed and stored for further characterization.

Table 1. Samples labels and parameters used for the experimental design of the ZnO growth.

.

Label	Temperature (°C)	Pressure (torr)	Zn mass (mg)
S0	750	10	50
S1	750	10	100
S2	750	760	50
S3	750	760	100
S4	950	10	50
S5	950	10	100
S6	950	760	50
S7	950	760	100

2.2. Synthesis and incorporation of AgNPs on the ZnO

Figure 1 exhibits the main elements of the experiment used for the silver nanoparticle synthesis. The system consists of two Ag electrodes (1.5 mm) immersed 80 mm into distilled water. A power source with an electronic control provides voltage, with alternating polarity between the Ag electrodes. To control the temperature of the reaction, a water bath monitored by a thermocouple was used.

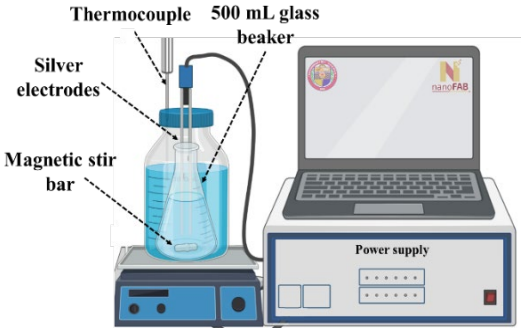

Fig 1. Illustration of the electrolysis system implemented for the synthesis of Ag NPs.

The current flowing through the Ag electrodes was measured using a source measure unit. The experiment was sustained 90 min at 80 °C, with a sweep voltage varied from 20 to 30 V with steps of 2 V. The Ag NPs colloids were labeled as nv1 to nv6. After ZnO synthesis, a micro-spraying system like the one presented in Figure 2, was used to incorporate the Ag NPs. The system was loaded with 120 mL Ag NPs for micro-spraying the ZnO surface at 35 °C.

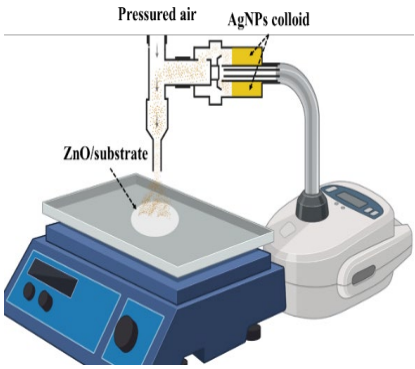

Fig 2. Schematic of a micro-spraying system for the incorporation of Ag NPs on the ZnO surface.

2.3. Materials characterization

Size measurement of Ag NPs was obtained by dynamic light scattering (DLS), using a Zsizer nano system model ZS DLS, equipped with a 632.8 nm red laser of 4 mW power. The absorbance of Ag NPs was obtained with a Thermo Scientific spectrophotometer model Multiskan GO, in a wavelength range from 300 - 700 nm and a step of 1 nm. The Ag NPs deposition process was characterized by means of an atomic force microscope JOEL model JSPM-4210 in non-contact configuration, using a HQ:NSC15/A1 BS cantilever. Surface morphology studies of the ZnO samples and Cathodoluminescence (CL) characterization were obtained by scanning electron microscopy (SEM) on a JEOL JSM 5300 equipment operating at 15 kV. CL spectra were obtained using a wavelength range of 200 nm to 900 nm. Electrical characterization was performed in a Keithley 4200-SCS Parameter Analyzer. X-ray photoelectron spectroscopy (XPS) of as-grown and Ag NPs decorated ZnO T-NWs were obtained by a K-Alpha Thermo Scientific equipment

with an Al Kα X-ray source, in an analysis area of 400 μm^2. The signals were adjusted at 284.8 eV of adventitious C 1s. The sample was cleaned by surface erosion using 1 kV argon ions for 15 s to remove surface impurities.

3. Results and discussion

3.1 Silver nanoparticles characterization

Figure 3 (a) shows the histograms of the particle size of each Ag NPs of the experiments proposed. The current through the electrodes versus time, and the relationship between the particle diameter and voltage curves, are presented in Figures 3 (b) and 3 (c), respectively. As can be observed, the Ag NP diameter is directly related with the applied voltage between the silver electrodes. Furthermore, a notorious increment in the current value was obtained, commonly produced by the electrolysis procedure. It can also be associated with the increased diameter of the nanoparticle from a mean value of 6.5 nm at 20V to 18.2 nm at 30 V.

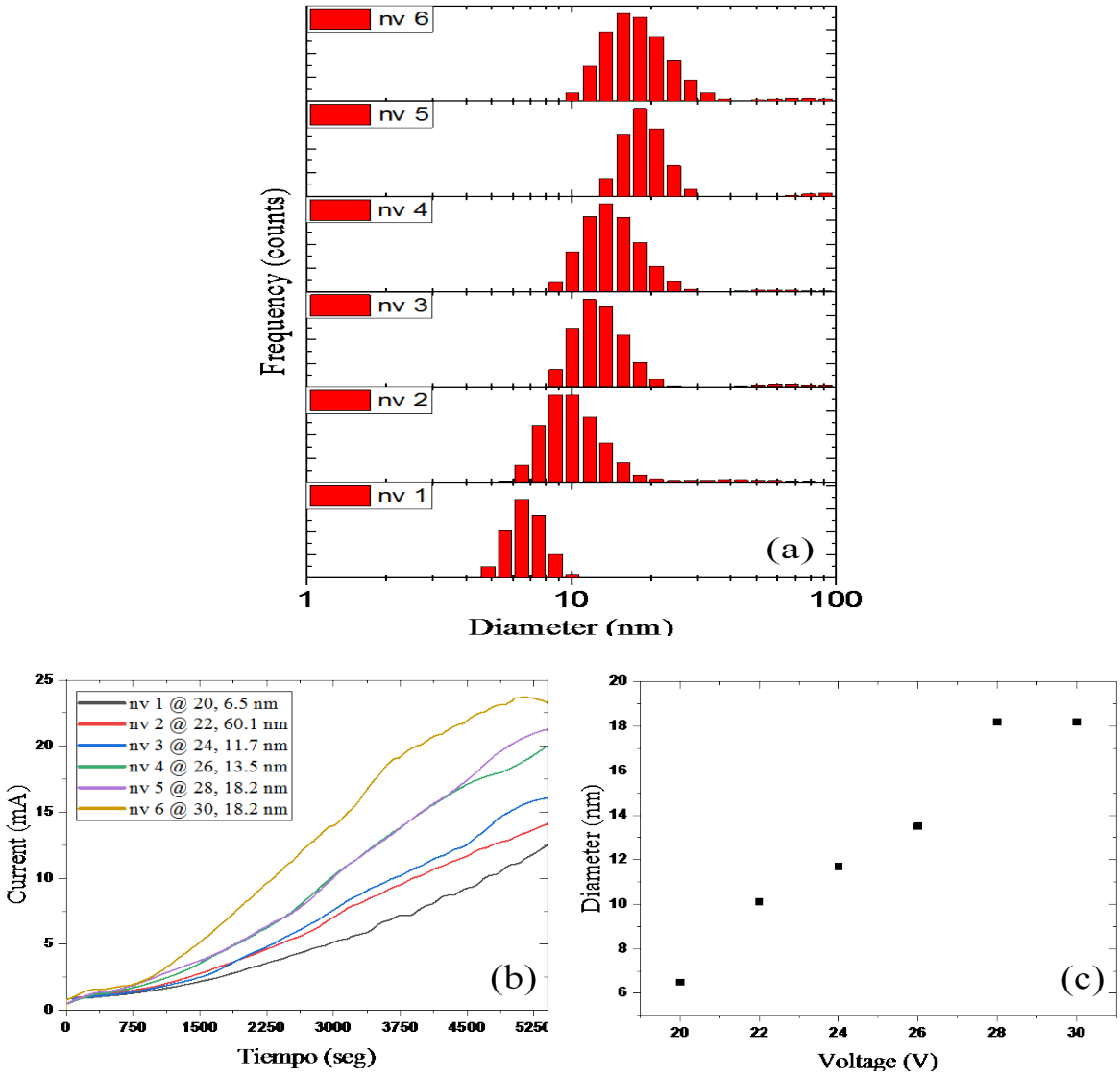

Fig 3. (a) Diameter distribution histograms of the synthesized Ag NPs. (b) Current in the system versus time. (c) Relation between diameter of Ag NPs and the applied voltage.

The absorbance spectra of Ag NPs are presented in Figure 4. As observed in all curves, the characteristic surface resonance plasmon localized at 413 nm was identified [21,22]. Despite the similitude in the optical response of surface plasmon resonances, a difference in the percentage of absorption was observed among Ag NPs. The latter can be attributed to the difference between the diameter and the shape of the nanostructures.

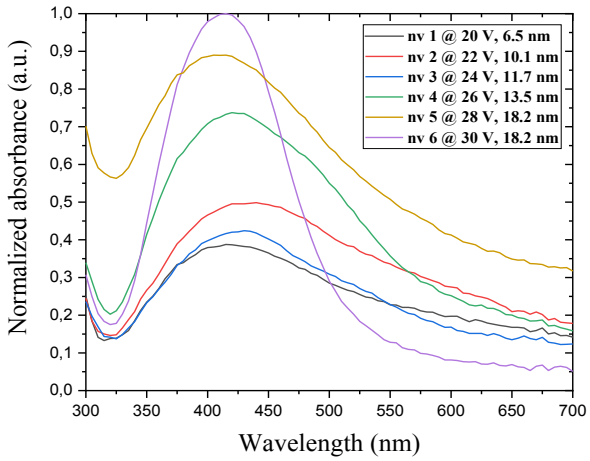

Fig. 4. Absorbance spectra of Ag nanoparticles synthesized by means of electrolysis.

3.2. Characterization of ZnO experimental design

Figure 5 shows the surface morphology obtained from the 2^3 experimental design, resulting in two variations of ZnO structures: nanodendrites and tip-like nanowires. A summary of the morphology and size as a function of the experimental factors is presented in Table 2. On the one hand, nanodendrites were mainly observed in experiments carried out at atmospheric pressure. This can be attributed to the slow growth rate of the ZnO due to the relatively high pressure, and the partial pressure reduction for Zn powder.

On the other hand, when ZnO was grown under 10 Torr, tip-like nanowires were obtained. From this experimental design, the most important growth parameter to obtain the wire morphology, was the pressure of the system as shown in samples S1, S4, and S5. Figure 6 presents the relation between the morphology and the experimental parameters. As observed, the curve in the pressure parameter exhibits the steepest slope, indicating the greatest influence on the ZnO structure morphology. Moreover, the inset in the Figure 6 shows the tendency for the tip-like nanowires formation as function of the temperature. Using this CVD methodology, T-NWs ZnO growth using a mass of 100 mg and a temperature of 750 °C, under a pressure of 10 Torr can be accomplished as observed in sample S1. In comparison, the production of larger structures was found at a temperature of 950 °C and a pressure of 10 Torr, as shown in samples S4 an S5 samples.

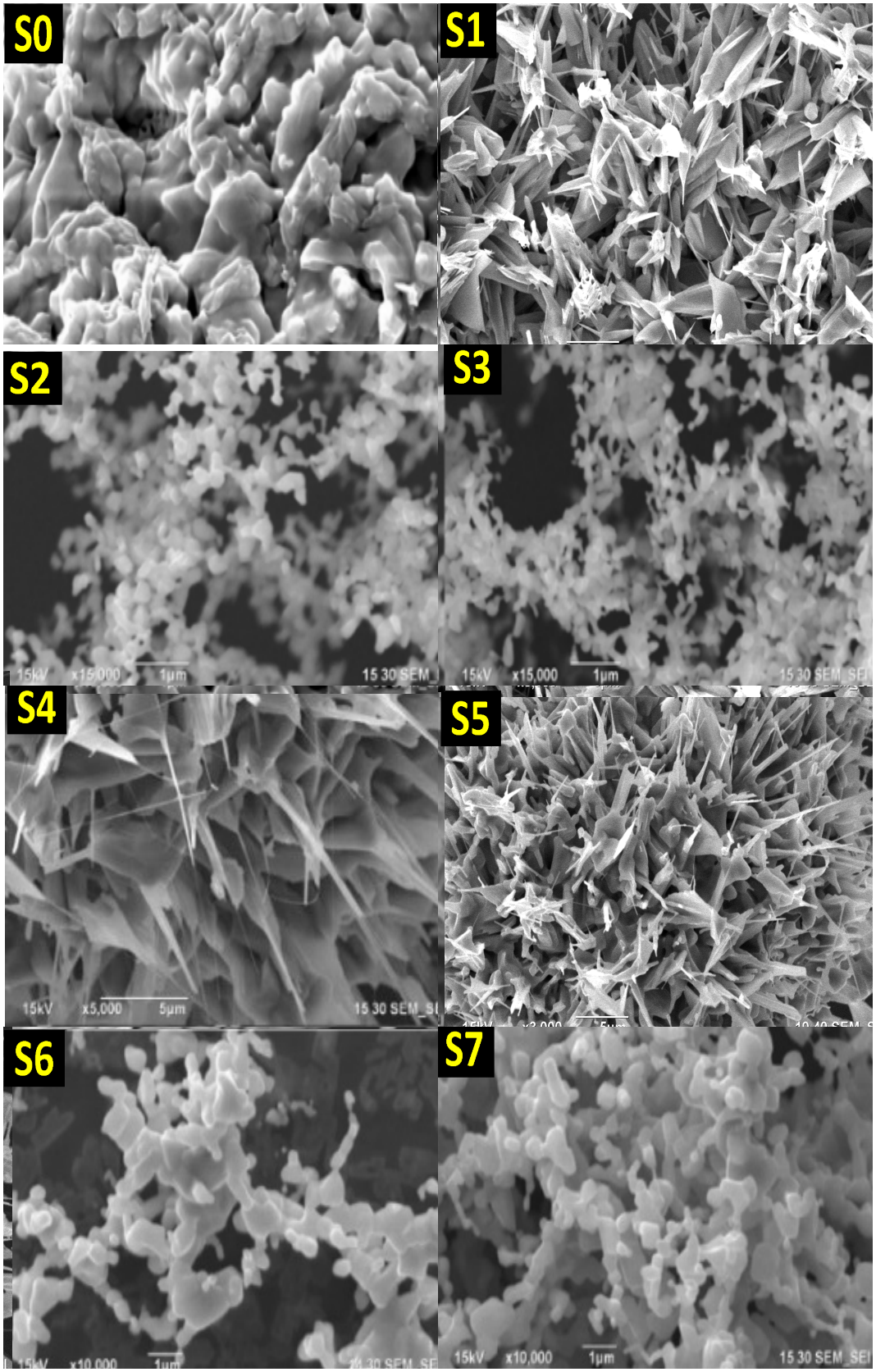

Fig 5. SEM images of ZnO grown in a CVD system under a 2^3 experimental design.

Table 2. Summary of the experimental design for the study of the ZnO structure.

Label	Temperature (°C)	Pressure (Torr)	Zn mass (mg)	Structure 0 – Nanodendrites 1 – Tip-like NW	Particle size (nm)
S0	750	10	50	0	1743
S1	750	10	100	1	335
S2	750	760	50	0	243
S3	750	760	100	0	215
S4	950	10	50	1	126
S5	950	10	100	1	442
S6	950	760	50	0	437
S7	950	760	100	0	435

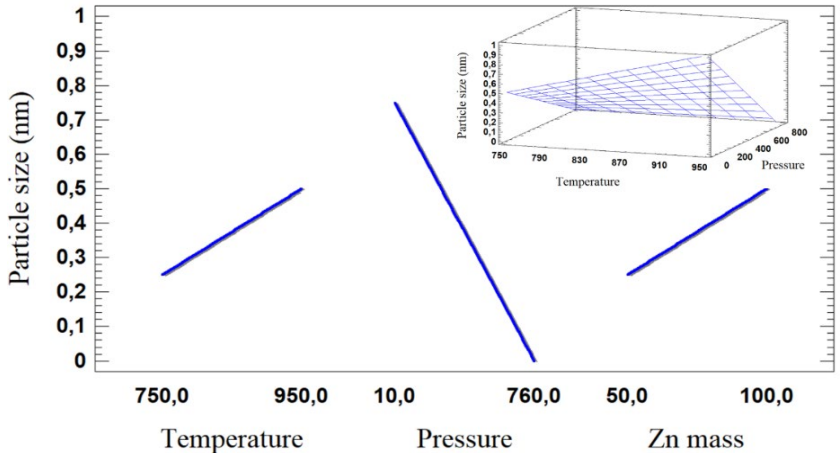

Fig 6. Principal effects in the experimental design of ZnO structures deposited by chemical vapor deposition.

Figure 7 shows the cathodoluminescence spectra of ZnO for each factorial experiment. The characteristic emission of ZnO was observed in all samples, which is composed of two bands at 370 nm and 500 nm, respectively. The first emission is related to an exciton-donor bound of ZnO while the band of lower energy is associated with intrinsic defects in the semiconductor such as oxygen vacancies at different depths [23].

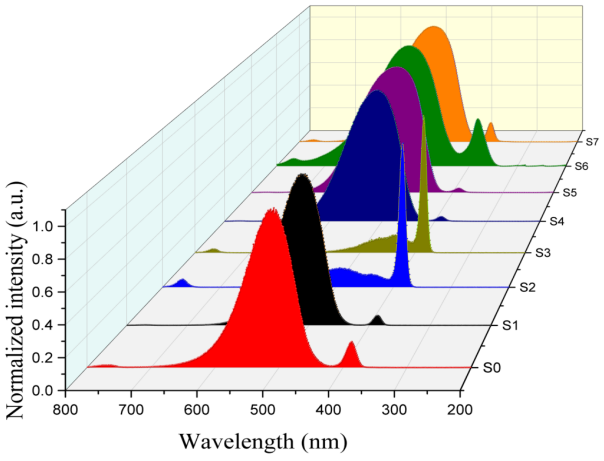

Fig 7. Cathodoluminescence emission of ZnO samples grown in a CVD system under an experimental factorial design.

The high-energy emission of the ZnO samples exhibits different CL intensities. As observed in Figure 7, samples S0, S1, S4, S5, and S7 show weak excitonic peak located at 370 nm instead to the strong emission at 500 nm. This attenuation in the luminescence has been previously reported to be suitable for the improvement of the gas sensing device, due to the difference in the surface properties/defects [24]. Based on the surface morphology and optical analysis, sample S4 was selected for the decoration of ZnO T-NWs using Ag NPs.

3.3. Characterization results of ZnO tip-like NWs decorated with Ag NPs

SEM images presented in Figure 8 show the presence of Ag nanoparticles on the surface of ZnO tip-like nanowires, deposited by the micro-spraying technique. Image analysis was used to determine the diameter of the Ag NPs. It should be mentioned that the size of nanoparticles is comparable to the diameter found in nv6 DLS results.

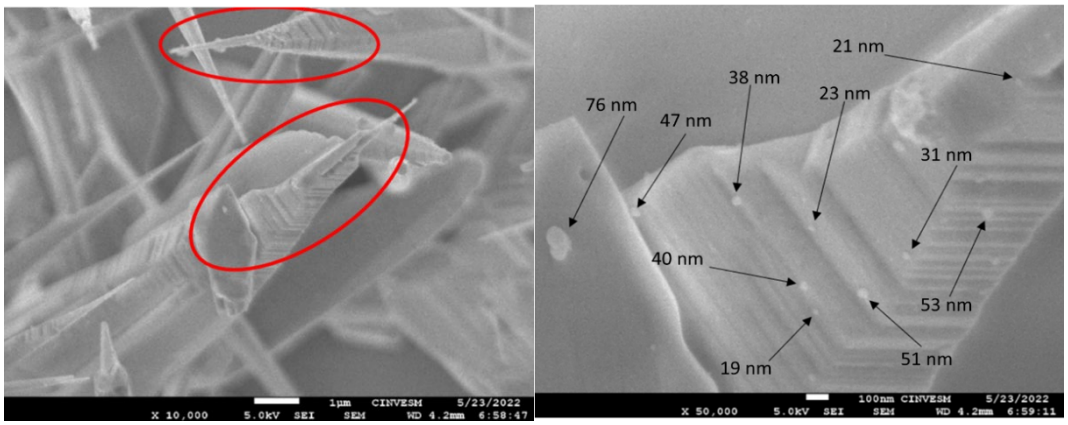

Fig 8. SEM images of silver nanoparticles on ZnO nanowires deposited by micro-spray technique.

Electrical measurements of Ag NPs-decorated ZnO were conducted at room temperature in a current range of ±12 µA. With the values obtained from the I-V measurements, the resistivity is calculated by applying current and measuring the voltage according to the four-point collinear method. Table 3, shows the main results of the electrical characterization. The results of the resistance value obtained from Figure 9 are presented. According to the parameters of the active films (F1: thickness, F2: separation between tips and F3: their position on the sample) an estimate of the factor of "F" correction is obtained. The F factor is not included in resistivity 1 while resistivity 2 considers it. Both values are an average obtained from the I-V curves of each measurement.

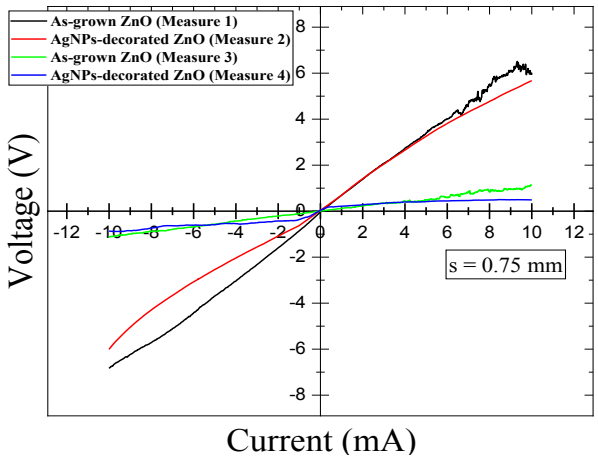

Fig 9. Electrical curves of the as-grown and AgNPs-decorated ZnO samples

The material containing the Ag NPs is more conductive according to the results obtained in the electrical characterization by at least 17.88%. This electrical response is suitable for gas sensing application due to the high sensitivity in electrical response as function of Ag NPs [25].

Table 3. I-V results of ZnO and Ag NPs/ZnO.

Measurement	R(kΩ)	F	Resistivity 1 (kΩ•cm)	Resistivity 2 (kΩ•cm)	**Δ**R1%	**Δ**R2%
1	711.9	0.026	335	8.72	-17.46 %	-17.88 %
2	587.6	0.026	275	7.16		
3	110.4	0.026	53	1.38	+27.71 %	+52.17 %
4	141.0	0.026	81	2.11		
Equation	$R = \frac{V}{I}$	$F = F_1F_2F_3$	$\rho = 2\pi s\frac{V}{I}$	$\rho = 2\pi sF\frac{V}{I}$		

To explore the potential in the application of Ag NPS-decorated ZnO T-NWs on the development of a gas sensing electronic device, the analysis of the chemical interaction between Ag nanoparticles and the surface of ZnO was performed by means of X-ray photoelectron spectroscopy. The survey spectra of both samples are presented in figure 10.

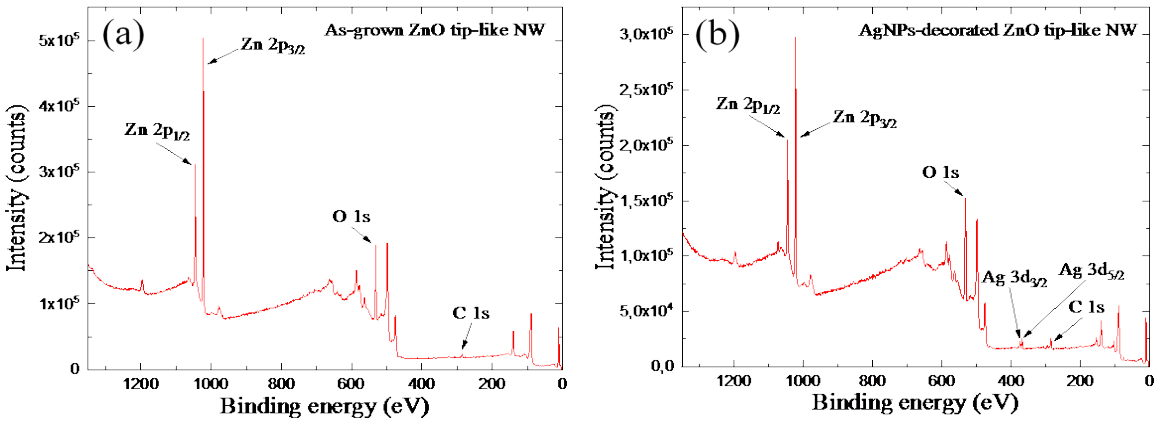

Fig 10. Survey XPS spectrum of as-grown and AgNPs-decorated ZnO samples.

As observed in the spectra of the as-grown and AgNPs-decorated ZnO samples, the strong signals Zn 2p and O 1s are observed in both samples, implying the majority ZnO chemical composition in the sample. However, a signal with lower intensity is observed in the AgNPs-decorated ZnO spectra, as exhibited in Figure 10 (b). This photoelectronic peak corresponds to the Ag 3d core level, produced by the Ag NPs on the ZnO surface. Despite the deposition of silver nanoparticles, the binding energy difference between the Zn $2p_{1/2}$ and Zn $2p_{3/2}$ is approximately 23 eV for both samples, as-grown and AgNPS-decorated ZnO. From this analysis, the decoration of ZnO with Ag NPs was confirmed. The calculated elemental composition of both samples is presented in Table 4.

Table 4. Elemental composition determined of as-grown and AgNPs ZnO.

Sample	O%	Zn%	Ag%	Zn/O ratio
As-grown ZnO	61.27	38.73	-	0.63
AgNPs/ZnO	72.67	24.70	2.63	0.34

Based on the results, the chemical composition of the as-grown ZnO exhibits an elemental Zn/O ratio of 0.63. However, with the presence of Ag NP, a decrease in the Zn/O was observed, being reduced to 0.34. This is related to the increment in the oxygen level in the sample, attributed to the interaction between ZnO surface and Ag NPs. This coupling promotes the formation of a stable silver oxide (Ag_2O) on the nanoparticles, due to the low dimensions of the nanoparticles and the high oxygen level in the as-grown ZnO. On further analysis, Figure 11 exhibits the deconvolution of high-resolution XPS spectra of the core levels Zn 2p, O 1s and Ag 3d and the summary of the results are presented in Table 5. Both Zn 2p and O 1s exhibits a shift to higher binding energy after the deposition of Ag nanoparticles on the ZnO nanostructures. Moreover, an increase in the intensity of the adjusted peak in O 1s at 531.55 eV was observed, commonly attributed to the O^{2-} oxygen deficient regions in matrix of ZnO [26].

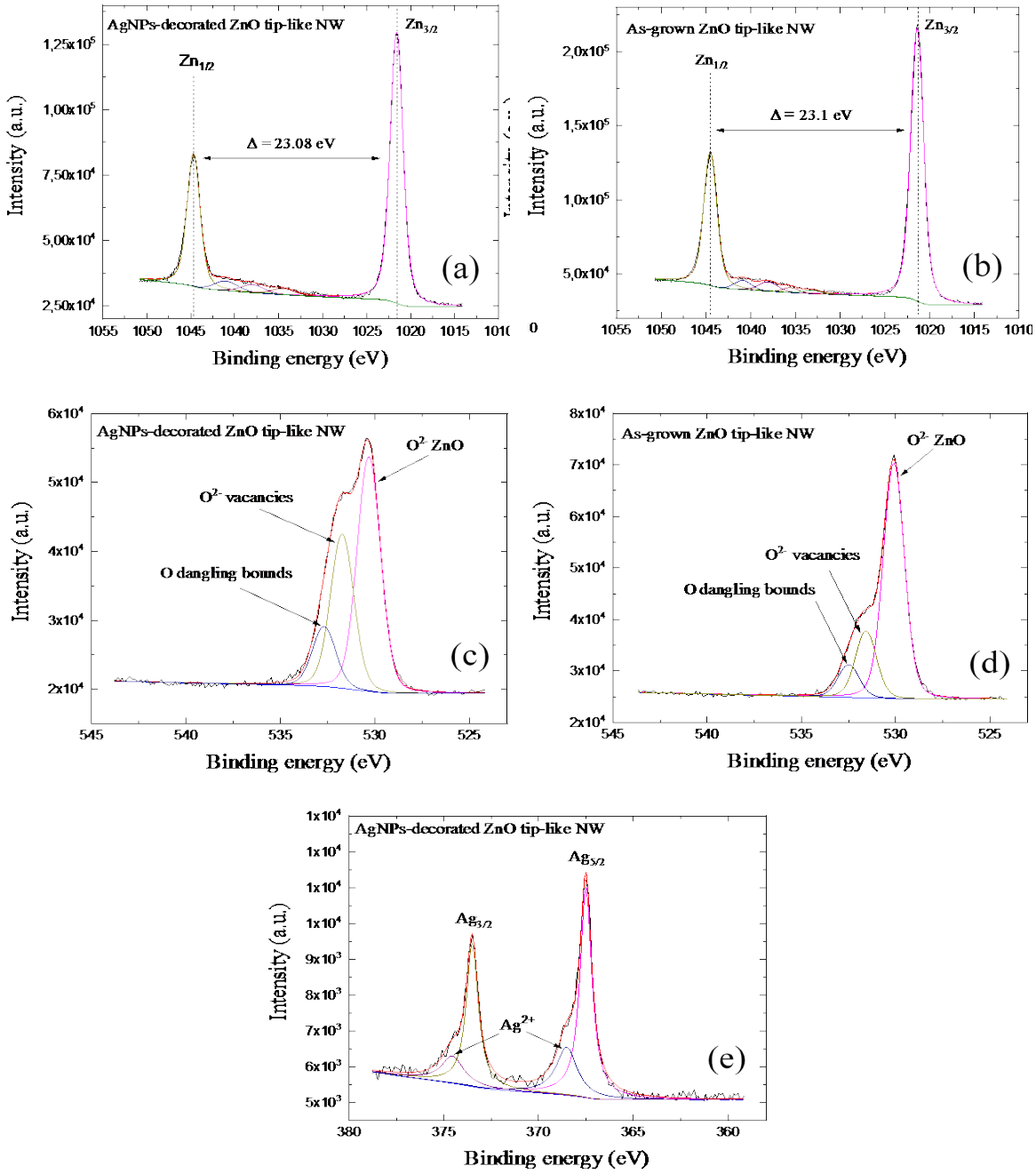

Fig 11. High resolution XPS spectra of core levels Zn2p, O1s and Ag3d of as-grown ZnO and AgNPs-decorated ZnO tip-like nanowires.

Table 5. Summary of binding energy of high-resolution XPS spectra.

Sample	O1s	$Zn2p_{1/2}$	$Zn2p_{3/2}$	$Ag3d_{3/2}$	$Ag3d_{5/2}$
As-grown ZnO	530.07	1021.37	1044.46	368.50	374.53
AgNPs/ZnO	530.30	1021.57	1044.66	-	-

The energy shift and the increment in the intensity of the fitted peak can be an indicator of O^{2-} charges being transferred from ZnO surface to Ag nanoparticles. Furthermore, an additional signal in the Ag 3d core level is notorious, as exhibited in Figure 11 (e), which is related to the

Ag^{2+} from the oxide phase Ag_2O [27,28]. The previous assumption is supported by the following mechanism. When silver nanoparticles are deposited on the surface of the semiconductor, the chemical interaction between these two materials produces the formation of a stable oxidation phase Ag_2O layer on the silver nanoparticles, as product of an oxidation reaction. As consequence, an increment of bridging oxygens between Ag-O-Zn occurs, enhancing the transference of charges in the ZnO T-NW due to a redox reaction from the Ag_2O. Based on this discussion, the increase in the electrical response from resistivity characterization can be highly related to charges exchange between ZnO and Ag nanoparticles. The latter mechanism is suitable for improving the charge transfer and electrical performance in ZnO-based gas sensors [29].

4. Conclusions

The synthesis of silver nanoparticles was successfully performed by a home-made electrolysis system. Additionally, DLS results denoted the control in the size of Ag NPs colloid as function of the supplied voltage in the silver electrodes. The characteristic surface plasmon resonance of Ag NPs located at 413 nm was identified by the absorption spectra. From the two-level factorial experimental design, the formation of ZnO tip-like nanowires was obtained, demonstrating that high temperature, low pressure, and low zinc mass are the essential parameters for the growth of this morphology. By cathodoluminescence, the characteristic emissions of zinc oxide at 370 and 500 nm were observed. The decoration of ZnO T-NWs with Ag NPs was accomplished by micro-spraying. SEM images provide evidence of the presence of Ag NPS on the semiconductor structures surfaces.

Additionally, electric characterization showed that silver nanoparticles enhance the electrical response of ZnO tip-like nanowires. X-ray photoelectron spectroscopy results indicates that charges-exchange mechanism is presented in the AgNPs-decorated ZnO. As consequence of a redox reaction between the nanoparticles and the semiconductor, the increase of charges obtained in the surface can be associated with the electrical response herein presented. The procedure performed in this work, opens up an opportunity to explore the application of AgNPs-decorated ZnO T-NWs for the improvement in gas sensors by applying these structures as active layer.

Acknowledgments

The authors gratefully acknowledge the support of nanoFAB Laboratory (272894), National Laboratory LaNNaFab (294452) and to the Internal Proyect DCEN (USO315007857). Also, UNISON for using its facilities and material provided to accomplish this work. J.V. Lopez-Fernandez acknowledges the scholarship provided by CONACYT.

References

[1] S.G. Leonardi, Chemosensors. 5(17), 7 (2017); https://doi.org/10.3390/chemosensors5020017

[2] J. Zhang, T. Liu, Y. Zhang, W. Zeng, F. Pan, X. Peng, Journal of Materials Science: Materials in Electronics, 26(3), 1347 (2015); https://doi.org/10.1007/s10854-014-2545-3

[3] P.I. Reyes, C.J. Ku, Z. Duan, Y. Lu, A. Solanki, K.B. Lee, Applied Physics Letters, 98(17), 173702 (2011); https://doi.org/10.1063/1.3582555

[4] S.J. Pearton, F. Ren, Current Opinion in Chemical Engineering, 3(2211), 51 (2014); https://doi.org/10.1016/j.coche.2013.11.002

[5] A. Wei, L. Pan, W. Huang, Materials Science and Engineering:B, 176(0921), 1409 (2011); https://doi.org/10.1016/j.mseb.2011.09.005

[6] Q.H. Li, Y.X. Liang, Q. Wan, T.H. Wang, Applied Physics Letters, 85(26), 6389 (2004); https://doi.org/10.1063/1.1840116

[7] C. Soci, A. Zhang, B. Xiang, S.A. Dayeh, D.P.R. Aplin, J. Park, X.Y. Bao, Y.H. Lo, D. Wang,

Nano Letters, 7(4), 1003 (2007); https://doi.org/10.1021/nl070111x
[8] H.T. Wang, B.S. Kang, F. Ren, L.C. Tien, P.W. Sadik, D.P. Norton, S.J. Pearton, J. Lin, Applied Physics Letters, 86(24), 1 (2005); https://doi.org/10.1063/1.1949707
[9] O. Lupan, G. Chai, L. Chow, Microelectronic Engineering, 85(0167), 2220 (2008); https://doi.org/10.1016/j.mee.2008.06.021
[10] S. Ananthi, M. Kavitha, E. Ranjith Kumar, T. Prakash, R. Vandamar Poonguzhali, B. Ranjithkumar, A. Balamurugan, C. Srinivas, D.L. Sastry, Inorganic Chemistry Communications, 146(1387), 110152 (2022); https://doi.org/10.1016/j.inoche.2022.110152
[11] O.W. Kennedy, M.L. Coke, E.R. White, M.S.P. Shaffer, P.A. Warburton, Materials Letters, 212(0167), 51 (2018); https://doi.org/10.1016/j.matlet.2017.10.017
[12] R. O'Haire, E. McGlynn, M.O. Henry, J.P. Mosnier, Superlattices and Microstructures, 42(0749), 468 (2007); https://doi.org/10.1016/j.spmi.2007.04.020
[13] A. Menzel, R. Goldberg, G. Burshtein, V. Lumelsky, K. Subannajui, M. Zacharias, Y. Lifshitz, Journal of Physical Chemistry C, 116(9), 5524 (2012); https://doi.org/10.1021/jp212635w
[14] P. Narin, E. Kutlu-Narin, S. Kayral, R. Tulek, S. Gokden, A. Teke, S.B. Lisesivdin, Journal of Luminescence, 251(0022), 119158 (2022); https://doi.org/10.1016/j.jlumin.2022.119158
[15] Z. Zhu, T.L. Chen, Y. Gu, J. Warren, R.M. Osgood, Chemistry of Materials, 17(16), 4227 (2005); https://doi.org/10.1021/cm050584
[16] M.H. Huang, Y. Wu, H. Feick, N. Tran, E. Weber, P. Yang, Advanced Materials, 13(2), 113 (2001); https://doi.org/10.1002/1521-4095(200101)13:2<113::AID-ADMA113>3.0.CO;2-H
[17] H.J. Fan, P. Werner, M. Zacharias, Small, 2(6), 700 (2006); https://doi.org/10.1002/smll.200500495
[18] P. Rai, Y.S. Kim, H.M. Song, M.K. Song, Y.T. Yu, Sensors and Actuators B Chemical, 165(0925), 133 (2012); https://doi.org/10.1016/j.snb.2012.02.030
[19] L. Wang, S. Wang, M. Xu, X. Hu, H. Zhang, Y. Wang, W. Huang, Physical Chemistry Chemical Physics, 15(40), 17179 (2013);https://doi.org/10.1039/c3cp52392f
[20] L. Xu, R. Xing, J. Song, W. Xu, H. Song, Journal of Materials Chemistry C, 1(11), 2174 (2013); https://doi.org/10.1039/c3tc00689a
[21] S.H. Jeong, H. Choi, J.Y. Kim, T.W. Lee, Particle Systems Characterization, 32(2), 164 (2015); https://doi.org/10.1002/ppsc.201400117
[22] M. Ider, K. Abderrafi, A. Eddahbi, S. Ouaskit, A. Kassiba, Journal of Cluster Science, 28(3), 1051 (2017); https://doi.org/10.1007/s10876-016-1080-1
[23] K. Vanheusden, W.L. Warren, C.H. Seager, D.R. Tallant, J.A. Voigt, B.E. Gnade, Journal of Applied Physics, 79(10), 7983 (1996); https://doi.org/10.1063/1.362349
[24] T.A. Thu Do, H.T. Giang, D. Van Huong, P.Q. Ngan, G.H. Thai, D.T. Thu, T.D. Lam, RSC Advances, 7(16), 9826 (2017); https://doi.org/10.1039/C6RA27737C
[25] A.S.M. Iftekhar Uddin, D.T. Phan, G.S. Chung, Sensors and Actuators B Chemical, 207(0925) 362 (2015); https://doi.org/10.1016/j.snb.2014.10.091
[26] J. Wang, Z. Wang, B. Huang, Y. Ma, Y. Liu, X. Qin, X. Zhang, Y. Dai, ACS Applied Materials and Interfaces, 4(8), 4024 (2012); https://doi.org/10.1021/am300835p
[27] G. Schön, J. Tummavuori, B. Lindström, C.R. Enzell, C.R. Enzell, C.-G. Swahn, Acta Chemica Scandinavica, 27(7), 2623 (1973); https://doi.org/10.3891/acta.chem.scand.27-2623
[28] L. Zhou, G. Zou, H. Deng, Catalysts, 8(7), 1 (2018); https://doi.org/10.3390/catal8070272
[29] Q. Xiang, G. Meng, Y. Zhang, J. Xu, P. Xu, Q. Pan, W. Yu, Sensors and Actuators B Chemical, 143(0925), 635 (2010); https://doi.org/10.1016/j.snb.2009.10.007